Available online at www.sciencedirect.com
SCIENCE DIRECT
Polymer 46 (2005) 4230–4241
polymer
www.elsevier.com/locate/polymer

Propagating waves of network formation induced by light☆

João T. Cabral*, Jack F. Douglas*

Polymers Division, National Institute of Standards and Technology, Gaithersburg MD 20899, USA

Available online 10 March 2005

Dedicated to Professor James E. Mark on the occasion of his 70th birthday.

Abstract

The exposure of a photopolymerizable liquid (e.g., multifunctional thiol-ene) to ultraviolet radiation often leads to a propagating wavefront of network formation that invades the unpolymerized material from the illuminated surface of the photosensitive material. We theoretically describe this light-driven frontal photo-polymerization (FPP) process, which is the basis of many commercially important fabrication methods, in terms of an order parameter $\phi(x,t)$ characterizing the extent of monomer-to-polymer conversion, the temporally and spatially evolving optical attenuation $\mu(x,t)$ of the medium, and the height $h(t)$ of the resulting solidified material. The non-trivial aspects of this frontal polymerization process derive from the coupling of $\mu(x,t)$ and the growing non-uniform network $\phi(x,t)$ and we consider limiting situations in which the optical attenuation increases ('photodarkening') or decreases ('photobleaching') in time to illustrate the general nature of FPP front propagation and the essential variables on which it depends. Since FPP fabrication of complex three-dimensional structures containing components having different material characteristics would greatly extend the practical utility of this method, we explore the influence of nanoparticle (silica, titania, and multi-wall carbon nanotube) additives on FPP front propagation. We also characterize the influence of temperature on the kinetics of FPP since this factor can often be controlled in practice. The experiments elucidate basic physical aspects of FPP and are well described by our model with a sensible variation of relevant physical parameters (optical attenuation and chemical rate constant) governing frontal growth. Our results are of interest both from the standpoints of complex structure fabrication and for understanding the fundamental nature of the FPP process.
Published by Elsevier Ltd.

Keywords: Frontal photopolymerization; Field theory model; Optical attenuation

1. Introduction

It is common practice to form solid network materials by photopolymerization. The conversion process from a liquid to a solid does not occur uniformly in this fabrication technique because of the attenuation of light within the photopolymerizable material (PM) and this process is normally accompanied by non-uniform monomer-to-polymer conversion profiles perpendicular to the illuminated surface [1–4]. Physically, these conversion profiles propagate as travelling waves of network solidification that invade the uncross-linked medium exposed to ultraviolet (UV) radiation if the process occurs in the presence of strong optical attenuation and limited mass and heat transfer. The frontal aspect of the polymerization process is apparent in the photopolymerization of thick material sections and has counterparts in degradation (including discoloration) processes in polymer films exposed to UV radiation where the breaking rather than the formation of chemical bonds is often the prevalent physical process. Frontal photopolymerization (FPP) is a versatile method of polymer synthesis. This type of solidification process is widely used in diverse fabrication processes, ranging from photolithography of microcircuits to dental restorative and other biomedical materials, and numerous coatings applications (paints and varnishes, adhesives and printing inks) [4]. We have recently explored the use of FPP in the fabrication of microfluidic devices [5,13].

At the outset, we emphasize that FPP is a distinct mode of polymerization from thermal (TFP) and isothermal (IFP) frontal polymerization, which are autocatalytic reaction processes. While these polymerization methods also involve

☆Contribution of the National Institute of Standards and Technology, not subject to copyright in the United States.

* Corresponding authors.
E-mail addresses: joao.cabral@nist.gov (J.T. Cabral), jack.douglas@nist.gov (J.F. Douglas).

0032-3861/$ - see front matter Published by Elsevier Ltd.
doi:10.1016/j.polymer.2005.02.052

wavelike polymerization fronts, the front propagation is sustained by the thermal energy released from an exothermic polymerization reaction. In TFP, the reaction is initiated by a localized heat source and the rate of front propagation is governed by both the rate of thermal diffusion and the nonlinear T dependence of the polymerization rate constants. In IFP, polymerization occurs in a viscous fluid or gel matrix that inhibits chain termination (Trommsdorff or 'gel' effect) and the reaction develops into self-sustaining front through the introduction of a 'seed', much like a crystallization front in a super cooled liquid initiated by introducing a nucleating agent. Pojman et al. [6] reviewed these autocatalytic frontal polymerization reactions.

A number of photoinitiation and FPP models have been recently reported in the literature [7–13] Some treatments account for photochemical reaction details with various degrees of complexity, including initiator photolysis, chain initiation, propagation and termination. Particular emphasis has been given in the past to following the evolution of photoinitiator concentration in the special case of photobleaching radical polymerization. Some of these previous treatments include additional diffusion mechanisms for the monomer [10] or initiator [8,11] and particular mass and or heat transfer processes [10,12] that occur in conjunction with photopolymerization. The utilization of such models requires the determination of numerous parameters describing the kinetic coefficients and transport properties, and their coupling as these variables are changed.

Given the complexity of these systems, we seek to utilize a 'minimal' FPP model based on physical observables relevant to fabrication processes utilizing this method. In particular, we are concerned with two basic FPP characteristics and their evolution in time: (1) the position of the solid/liquid front, which defines the patterned height and (2) the light transmission of the PM layer. Our model involves a system of coupled partial differential equations describing the extent of monomer-to-polymer conversion, $\phi(x,t)$, and the light attenuation $\mathrm{Tr}(x,t)$ as a function of the distance from the illuminated surface x and time t.

Before describing our mathematical model, we illustrate the physical nature of FPP through some concrete examples of this fabrication method in Section 2. The parameter space requiring exploration is large so we adopt a combinatorial approach to cover this parameter space efficiently. Since, the light attenuation Tr and exposure time t or ('dose') are basic control variables for FPP, we construct an array of photopolymerization fronts of common cross-sectional shape, where each front is developed for a fixed t and Tr. (A previous paper explored the influence of varying the formulation of the thiol-ene PM[13]). The effect of temperature and its significance to front propagation is also explored with combinatorial experimentation. Moreover, since it is attractive to form complex multi-component three-dimensional objects by this method, it appears relevant to modify the mechanical, thermal and electrical properties of the polymerized material. This region of the parameter space governing FPP is briefly explored by adding nanoparticles of various types to the photo-polymerizable material. Silica, titania and carbon nanotubes are taken to be representative particles that are widely appreciated to modify mechanical, optical and electrical properties and we thus focus on these widely available and utilized filler materials. In these initial nanoparticle studies, we are primarily concerned about whether it is possible to generate FPP fronts as in the unfilled material and, if so, whether the theoretical framework, developed for the PM alone, provides an acceptable description of the photo-polymerization of these complex mixtures.

Photo-polymerization front movement depends sensitively on the optical attenuation of the medium and its evolution after exposure to UV radiation. Since these properties can vary widely with the photopolymerizable material, temperature, additive composition, etc., we treat various cases that arise in practice in Section 4—the optical attenuation of medium decreases (photobleaching), increases (photodarkening) or remains unchanged (photo-invariant polymerization) with irradiation. Our analysis indicates that the FPP fronts can propagate with a constant velocity over long times when photobleaching is prevalent, but logarithmic front displacement dominates in the case of photodarkening. Some of these types of photopolymerization have been investigated experimentally and approximately analytically by Rytov et al. [7].

The FPP model is compared to the combinatorial time–temperature study and nanoparticle filler experiments in Section 5. This comparison shows that the FPP model is remarkably robust, with the T and the filler particles changing the rate constant for the FPP reaction and the average optical properties of the medium. Even in the extreme case of multi-wall carbon nanotubes, we found that we could effectively photopolymerize the nanoparticle filled polymer matrix, although the thickness was limited by the large optical attenuation of carbon nanotubes.

2. Experimental

2.1. Materials and equipment

We utilize a multifunctional thiol-ene based pre-polymer (optical adhesive 81, Norland Products) as model photopolymerizable material (PM) for this study. The thiol-ene PM is optically clear, UV curable at 365 nm (UVA), has a relatively low viscosity (3 Pa s) and a good adhesion to glass and metal surfaces. Multifunctional thiol-enes can be UV photopolymerized into highly cross-linked solid structures [15,16] at ambient conditions, with minimal oxygen inhibition. FFP kinetics of the neat system have been characterized at room temperature [13]. In this work, we investigate the effect of temperature and of the addition of nanoparticles. Three representative nanoparticle types were considered: fumed amorphous silica Aerosil OX 50 (40 nm

SiO_2 hydrophilic particles) and fumed titania Aeroxide P 25 (21 nm TiO_2 hydrophilic particles) were obtained from Degussa; multiwall carbon nanotubes CNT (grown by catalytic decomposition of hydrocarbons in a chemical vapor deposition reactor [17]) were kindly donated by Eric Grulke (University of Kentucky). Composite liquid mixtures were prepared by mechanically stirring 0.01–1% (mass fraction) of nanoparticles into the neat PM, followed by sonication at 45 °C for 24 h using a tabletop 40 kHz sonicator Bransonic 1510 (Branson). Mixture homogeneity was found to be satisfactory by optical microscopy [14].

2.2. Combinatorial photopolymerization

The experimental setup [14] is depicted in Fig. 1. It consists of a long wavelength UVA source, a photomask, and the PM confined between two surfaces separated by a gasket. The UV source is a 365 nm Spectroline SB-100P flood lamp, equipped with a 100 W Mercury lamp (Spectronics), and placed 50 cm from then specimens. Photomasks consisted of 10×10 or 3×9 arrays of transparent squares (2 mm×2 mm) on a black background. The thiol-ene PM works as a negative photoresist and, therefore, imaged areas become insoluble upon sufficient optical exposure ('development'). The masks were designed with Canvas 7.0 (Deneba) and printed on transparencies (CG3300, 3 M) using a black&white Laserjet 8000N printer (Hewlett Packard). The bottom surface was a 10 cm silicon wafer (4 inch, Wafer World), chosen for its high thermal conductivity, and the top surface was a transparent glass slide (75 mm×50 mm×1 mm, Corning 2947). Both surfaces were cleaned using an oxygen plasma (Anatech-SP100) for 3 min at 60 W prior to use. The gasket material was cut from a 3 mm thick slab of thermally cross-linked poly(dimethylsiloxane) elastomer (Sylgard 184, Dow Corning). The PM was poured onto the silicon surface to fill in the gasket material, and then covered with a glass slide. The assembly was placed on the temperature stage and the photomask applied.

Our temperature gradient stage [18] consists of an aluminum plate equipped with a moveable heat source and heat sink, and insulated with ceramic (Macor) supports. We use a VWR 1165 heated/refrigerated circulator as the cold source and a 200 W cartridge heater with a Micromega CN77000 controller (Omega) as the heat source. The individual heat source/sink temperatures were set to be identical for isothermal experiments and were different during gradient temperature (ΔT) experiments. The sample temperature across the stage was measured using a surface thermocouple (type K, CO1 Omega) with a Fluke 52 thermometer and a non-contact infrared thermometer (Oakton).

Photopolymerization was carried out under a fume hood, with a light intensity of (210–250) μW/cm^2. Using manual sliding shutters over the photomask, exposure times of the square slits in the array were varied in steps, yielding discrete UV dose intervals across individual samples. Combinatorial temperature/dose arrays (a 'library') were produced by imposing a temperature gradient orthogonal to the exposure time discrete steps, as indicated in Fig. 1. The UV dose (J/cm^2) $\equiv \mathrm{Tr}I(x=0)t$ administered to each slit was computed from the incident light intensity $I(x=0)$ (W/cm^2), exposure time t (s) and transmission Tr of the optical mask and glass slide [Tr(mask) ≈ 80% and Tr(glass) ≈ 94%]. The light intensity was measured with a digital radiometer Spectroline DRC-100X equipped with a DIX-365A UV-A sensor (Spectronics) before and after each experiment. Standard dose uncertainties are less than 5%, due to instrument resolution and intensity fluctuation. After UV exposure, the pattern was developed with a solvent rinse (acetone and ethanol) and by gently blowing compressed air (or nitrogen gas), thoroughly removing uncross-linked material. The remaining gel-like, percolated structure was then flood exposed to UV light, for a dose approximately 50 times the first, fully cross linking the material into a hard solid with ≧1 GPa modulus. An optional thermal cure at 50 °C for 12 h enhanced the adhesion to the glass substrate.

The topography of the photopolymerized patterns was evaluated by profilometry, using a Dektak 8 profilometer (Veeco, CA), equipped with a 12.5 μm stylus and operating

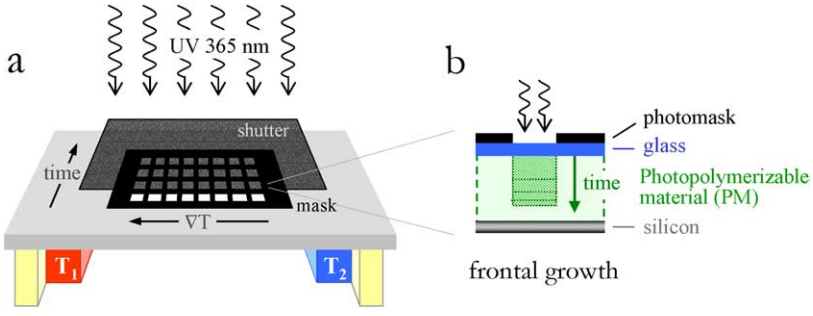

Fig. 1. Schematic of the experimental setup showing the collimated UV source, photomask, photopolymerizable material (PM) and confining surfaces (glass and silicon, in this case). (a) Combinatorial approach for investigating photopolymerization kinetics, involving a temperature gradient and an orthogonal UV exposure gradient. The temperature stage is equipped with a heat source and a heat sink, which maintain a linear T-gradient. A sliding shutter over the photomasks generates discrete light exposure steps. (b) Cross-section of panel (a) illustrating the growth of a polymerization front induced by light, orthogonal to the photomask.

at 10 mg force and 500 μm/s scanning speed. For patterned heights above 1 mm (beyond profilometer's height range), a digital caliper (Digit-cal MK IV, Brown & Sharpe) was employed. Measurement uncertainty is better than 5%, as estimated by one standard deviation.

The time evolution of the transmission of the neat thiol-ene PM during photocuring was investigated in real time. Sheets of prepolymer, with thicknesses from 90 μm to 1 mm, were confined between glass slides and allowed to photopolymerize between the UV source and radiometer. The sample transmissions (measured at 20 °C) were computed from the Beer–Lambert law, taking into account the attenuation of the glass slides: $\mathrm{Tr}(x) \equiv I(x)I(x=0)^{-1}\mathrm{Tr}(\mathrm{glass})^{-2} = \exp[-\mu(t)x]$.

3. Frontal polymerization induced by Light

We first establish the basic nature of the frontal photopolymerization (FPP) with some examples. Fig. 2 shows micrographs of arrays of FPP fronts grown in the form of a square (2 mm × 2 mm) cross-section. A combinatorial array of front samples is shown in Fig. 2(a), in which 100 exposure conditions, defined by temperature and UV dose, are evaluated. A temperature gradient, from right to left, was applied using a heat source and a heat sink separated by a conductive metal plate, which supports the PM. The temperature field was measured and T was assumed constant in each patterned region. The time exposure steps were fixed by a manual sliding shutter, orthogonal to the T-gradient. The interface between the polymerized solid and the liquid pre-polymer, characteristic of frontal polymerization, is evident after 'development' (selective washing away of the unpolymerized material). A representative isothermal ($T = 23.5$ °C) series of fronts, produced with UV doses ranging from 4 to 300 mJ/cm^2, is magnified in Fig. 2(a) (right panel). The dashed square indicates a feature that received the minimum dose (4 mJ/cm^2) which was washed away upon development, suggesting a 'threshold' UV dose for frontal growth. (Our model of frontal photopolymerization, described in the next section, predicts such a threshold.) The combinatorial library also shows that growth is viable at slightly higher temperatures, with the same UV dose. These results are discussed later in light of our FPP model.

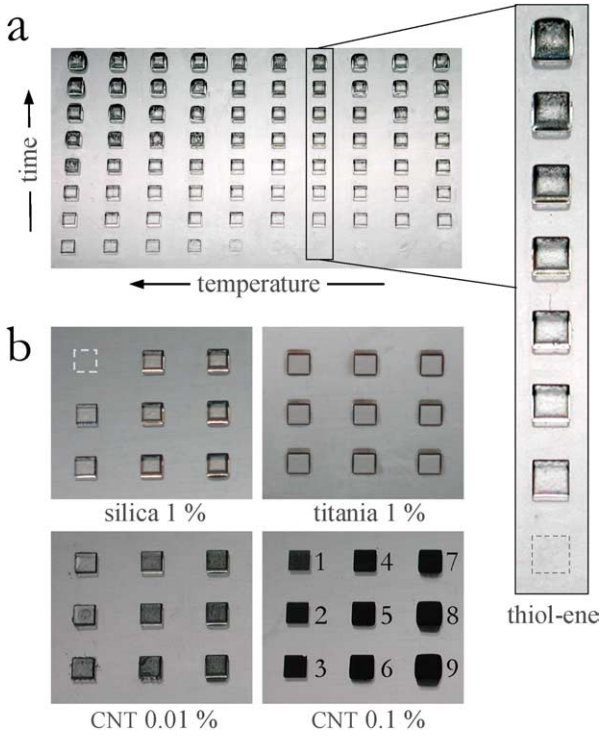

Fig. 2. (a) Combinatorial frontal photopolymerization patterns generated by varying the exposure time (bottom to top) and temperature (right to left) through an imposed photomask/shutter and T-gradient. The top panel shows an array of the neat thiol-ene PM exposed to UV dose 4–300 mJ/cm^2 (corresponding to exposure times of 30 s to 36 min at 230 mW/cm^2) on a linear T-gradient spanning 16–35 °C. The inset (right panel) magnifies the sample series corresponding to 23.5 °C; the dashed square indicates a pattern washed away during development (falling below a necessary critical dose). (b) The bottom four panels show a detail of polymer/nanoparticle arrays photopolymerized isothermally (20 °C) with increasing UV dose. Particle loading ranges from 0.01 to 1 mass fraction, as indicated. A double sliding shutter, consisting of two orthogonally stacked light blocking sheets, generates discrete light exposures (numbered). The patterned structures are 2 mm × 2 mm squares of various heights (20 μm to 1.6 mm).

Fig. 2(b) demonstrates that FPP fronts can be used to solidify samples with various dispersed nanoparticles. The optical and mechanical properties of these composite photopolymerized materials are clearly modified from the thiol-ene matrix, thus verifying that fillers can be incorporated into FPP to good practical effect.

These results demonstrate that the patterned height $h(t)$ is a function of the UV dose (or exposure time), temperature, and optical attenuation constant (altered by the nanoparticles). This feature dimensions (including the height) are, however, largely insensitive to the development procedure, implying a sharp solid–liquid boundary [13], expected for a frontal process. Fig. 3 shows profiles of FPP fronts after different exposure times for the neat thiol-ene PM and a filled composite (1% mass fraction) with titania nanoparticles. We observe that while the rate of FPP growth is significantly diminished, the sharpness of the FPP features is largely preserved in the presence of the nanoparticles.

4. Frontal photopolymerization (FPP) model

Photopolymerization begins with the absorption of light, which generates the reactive species responsible for chain initiation. The addition of a strongly light-absorbing photoinitiator modifies the optical properties of the medium and its consumption in the course network formation, in conjunction with network formation and the formation of photopolymerization by-products, leads to an evolving optical attenuation. The consumption of the photoinitiator

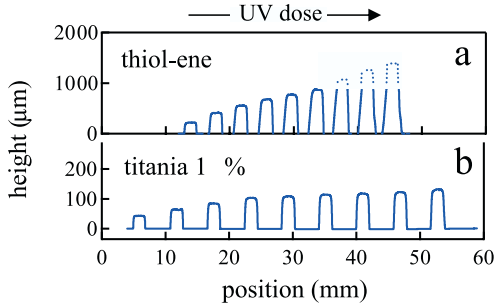

Fig. 3. Comparative FPP front profiles as a function of dose for the photopolymerized thiol-ene PM with and without nanoparticle additives, obtained by stylus profilometry. (a) Neat thiol-ene array, corresponding to the inset of Fig. 2(a) (23.5 °C); the UV dose ranges from 4 to 216 mJ/cm^2, yielding structure heights of (0–1200) μm. The patterns shown with dashed lines correspond to heights exceeding 900 μm (the profilometer vertical range), where the front position was determined with a caliper. (b) Profilometer scan along an array of patterned photopolymer loaded with 1% titania nanoparticles, corresponding to UV doses of 16–440 mJ/cm^2 resulting in structures 40–130 μm height. The absorption and scattering due to the particles slow down the growth, but the sharpness of the features is largely preserved for patterns at these length scales.

alone can be expected to lead to a reduction of the optical attenuation in the UV frequency range ('photobleaching'), but the resulting polymer network can have an increased optical attenuation so that the net optical attenuation can increase upon photopolymerization ('photodarkening'). Moreover, the addition of nanoparticle additives will also change the optical properties of the medium from those of the unfilled material in a non-trivial fashion. We thus develop a model of photopolymerization that does not presume either photobleaching or photodarkening as a general consequence of photopolymerization. The nature of the polymerization front development has distinct features in these physical situations that we discuss in separate sections below after summarizing our general model.

As mentioned earlier, a number of photopolymerization models have recently addressed the complex chemistry and reaction kinetics of FPP [1–4,7–12]. Since a full description of this chemistry is difficult, especially in commercial PM formulations where the composition is somewhat uncertain, we instead opt for a coarse-grained photopolymerization model [13]. Our model presumes that the state of the material is governed primarily by the existence of polymerized and unpolymerized material in the PM and the change in average optical properties that result from photopolymerization. While our model has mathematical similarities with classic theories of photo-polymerization [19,20], it directly focuses on observable properties of FPP rather than the concentration of the various chemical species involved. In particular, our main variables of interest are the FPP front position $h(t)$, as defined, for example, by the solid/liquid interface, the light transmission $\mathrm{Tr}(x,t)$ of the PM layer and the optical attenuation constants (μ_0, μ_∞) of the monomer and the fully converted material, respectively.

Our coarse-grained description of the photopolymerization front propagation is developed in a parallel fashion to previous phase-field descriptions of ordering processes such a crystallization and dewetting where propagating fronts are also observed [21,22]. The extent of polymerization $\phi(x,t)$ is then introduced as an 'order parameter' describing the extent of conversion of the growing polymerization front. The field variable $\phi(x,t)$ describes the average ratio of photopolymerized to unpolymerized material at a depth x (the illuminated surface $x\equiv 0$ defines the coordinate origin) into the PM and satisfies the limiting relations $\phi(x,t\to 0)=0$ (no polymer) and $\phi(x,t\to\infty)=1$ (i.e., full polymerization) for all $x>0$. The second field variable $\mathrm{Tr}(x,t)$ describes the average optical transmission of the photopolymerizable medium.

We model the evolution of the photopolymerization process by introducing appropriate rate laws. The rate of change of $\phi(x,t)$ is taken to be proportional to the light intensity $I(x,t)$ [J cm^{-2}], the amount of material available for conversion $1-\phi(x,t)$ and the reaction conversion rate K [cm^2 (Js)$^{-1}$],

$$\frac{\partial\phi(x,t)}{\partial t} = K[1-\phi(x,t)]I(x,t). \tag{1}$$

Once photopolymerization has commenced, the material is considered to be a two-component system (consisting of reacted and unreacted material) whose components do not generally have the same optical attenuation coefficient μ [mm^{-1}]. In our mean-field model, we take the material to be defined by a spatially varying and temporally evolving average optical attenuation, $\bar{\mu}(x,t)\equiv\mu_0[1-\phi(x,t)]+\mu_\infty\phi(x,t)$ where μ_0 and μ_∞ are the attenuation coefficients of the unexposed monomer (μ_0) and fully polymerized (μ_∞) material, respectively. The variation of $\bar{\mu}(x,t)$ leads to an evolution in the light intensity (or transmission) profile with depth according to the generalized Beer–Lambert relation,

$$\frac{\partial I(x,t)}{\partial x} = -\bar{\mu}(x,t)I(x,t), \tag{2}$$

where the usual Beer–Lambert law for a homogeneous material, $I(x)=I(0)\exp(-\bar{\mu}x)$, is recovered for short and long times as $\bar{\mu}(x,t\to 0)=\mu_0$ and $\bar{\mu}(x,t\to\infty)=\mu_\infty$.

The idealization of the FPP evolution modeled by Eqs. (1) and (2) neglects the fact that numerous chemical components are actually generated in the course of photopolymerization and ignores the presence of additives and impurities that are often present in the photopolymerizable material. Thus, it is not clear a priori whether such a simple order parameter treatment of FPP is suitable. Judgement of the adequacy of our approach must be decided by comparison to measurements performed over a wide range of conditions. We next consider the final basic observable property of the FPP process, the position of the photopolymerization front.

As in ordinary gelation, we can expect solidification to occur once ϕ exceeds a certain 'critical conversion fraction' ϕ_c ($\ll 1$). Since the liquid material can be simply washed

away after any exposure time, the height $h(t)$ at which $\phi(x,t)=\phi_C$ demarks the surface of the photopolymerized material after curing and washing. This defines the position of FPP front in a concrete way and we adopt it below. It should be appreciated that solidification by FPP involves a combination of gelation and glass formation effects since the glass transition of PM generally increases strongly with the degree of polymerization. This coupling of network formation and glass formation should influence the T dependence of ϕ_c and we explore this effect in Section 5.

Eqs. (1) and (2) define a system of non-linear partial differential equations whose solution depends on four material parameters: the short and long-time attenuation coefficients, μ_0 and μ_∞, the conversion rate KI_0 and the critical conversion ϕ_c. The former two parameters can be measured independently with a series of transmission measurements of uncross-linked and fully cross linked specimens of different thicknesses. K is determined by the polymerization chemistry and ϕ_c is a structural variable, yet both can be obtained as fitting parameters. The former has been the focus of much of the previous research [7–12,16,19,20], and is not discussed in the present paper. For convenience, we use dimensionless intensity, i.e., transmission $\mathrm{Tr}(x,t)\equiv I(x,t)/I_0$ of a layer of thickness x at time t to represent our results.

The coupled non-linear differential Eqs. (1) and (2) have not yet been solved analytically, apart from special limits that are briefly summarized in the next section. These exactly solvable cases include 'total photobleaching' where $\mu_0>0$ and $\mu_\infty=0$ and 'photo-invariant polymerization' in which the optical properties of the medium do not change in the course of polymerization (i.e., $\mu_0=\mu_\infty\equiv\bar{\mu}$). Front propagation is quite different in these different physical situations and we briefly describe the nature of FPP in these limiting regimes, as well as some other physically relevant cases (treated computationally because of the difficulty of analytic solution), to identify basic features of FPP that can be recognized experimentally. Rytov et al. [7] is one of few previous papers to study these different types of FPP, both by analytic modeling and experiment.

4.1. Total photobleaching ($\mu_0>0$, $\mu_\infty=0$)

The initiator of the photopolymerization reaction often absorbs light strongly and the absorption of radiation can expected to lead to a reduction of the optical attenuation upon UV radiation through the chemical degradation of this reactive species. If this were the only species contributing to the optical attenuation of the medium, then the photopolymerized material would become increasingly transparent to UV radiation, becoming perfectly transparent to the radiation at infinite times. This is evidently an idealized model of photopolymerized materials, but most theoretical discussions of photopolymerization [4,7–12] are restricted to this limiting case based on the assumption that the PM initiator dominates the optical attenuation.

The case of perfect optical absorption is one of the few limiting cases in which a limiting exact solution can be readily obtained and this solution is instructive into basic features of FPP. In this case, the PM has a positive attenuation constant ($\mu_0>0$) and the attenuation of the polymerized material equals, $\mu_\infty=0$. From Eqs. (1) and (2), the conversion fraction $\phi(x,t)$ for perfect photobleaching equals,

$$\phi(x,t) = [1-\exp(-KI_0t)]/[1-\exp(-KI_0t) + \exp(\mu_0x - KI_0t)], \quad (3)$$

which can be written equivalently in terms of the coordinate z of the moving front as,

$$\phi(x,t) = 1/[1+\exp(\mu_0 z)]; \quad (4a)$$

$$z = x - x_p, \quad x_p = \{KI_0t + \ln[1-\exp(KI_0t)]\}/\mu_0. \quad (4b)$$

The conversion fraction is only positive for $x>0$ so that $\phi(x,t)$ is implicitly multiplied by a Heaviside step function $H(x)$. Notably, the special solution of Eqs. (1) and (2) given by Eq. (3) was obtained long ago by Wegscheider [19], although the physical interpretation of these equations differs in his treatment which models the concentration of reactive species, rather than the extent of photopolymerization.

Eqs. (4a) and (4b) implies that $\phi(x,t)$ propagates as a moving sigmoidally-shaped front whose position is defined by x_p. At long times ($t\to\infty$), the front translates linearly in time with a constant rate KI_0/μ_0 so that the velocity of the frontal propagation is proportional to the photochemical reaction rate K and light intensity I_0, and is inversely proportional to the initial optical attenuation μ_0. We note that the conversion fraction is zero for $x<0$ for all time so that $\phi(x,t)=0$ for $t\to0^+$ since x_p approaches $-\infty$ in this limit. As time increases, the front position rapidly emerges from $-\infty$ and crosses into the positive x axis where $\phi(x,t)$ can be positive. From Eqs. (4a) and (4b), we see that this event occurs for the special time defined by the transcendental equation,

$$KI_0t = -\ln[1-\exp(-KI_0t)]/\mu_0. \quad (5)$$

The UV transmission $\mathrm{Tr}(x,t)$ is similarly exactly calculated as [23],

$$\mathrm{Tr}(x,t) = 1/[1-\exp(-KI_0t)+\exp(\mu_0x-KI_0t)], \quad (6)$$

This expression reduces to Beer–Lambert relation, $\mathrm{Tr}(x,t\to0^+)=\exp[-\mu_0(x)]$, for the photopolymerizable material at short times and $\mathrm{Tr}(x,t)$ frontally propagates into the medium with increasing time. [$\mathrm{Tr}(x,t)$ for air is unity in our model so that $\mathrm{Tr}(x<0,t)\equiv1$.] All of space thus becomes 'transparent' to UV radiation (i.e., $\mu=0$) in the limit of infinite times for total photobleaching, i.e., $\mathrm{Tr}(x,t\to\infty)=1$.

The location of the FPP front can be defined as the inflection point in $\phi(x,t)$, which is defined by the position of the (unique) maximum in $-\mathrm{d}\phi(x,t)/\mathrm{d}x=\phi_x$. By this

definition, the width of the front ξ can be correspondingly be defined as the reciprocal of the magnitude of ϕ_x at the front position,

$$\xi = 1/|\phi_x(\max)|. \tag{7}$$

This definition is suitable for any symmetric front shape for which $\phi(x,t) \approx ½$ at the inflection point and we note that $\phi(x,t)$ exactly equals ½ for total photobleaching. The front position can also be defined by $\phi(x,t)$ reaching some threshold value dictated by the physical nature of the material. This front definition [13] leads to a time translation of the front according to the same relation as Eqs. (4a) and (4b).

4.2. Photo-invariant polymerization ($\mu_0 > 0$, $\mu_\infty = \mu_0$)

Another important exactly solvable limit of our FPP model involves the situation in which the optical attenuation of the polymerized medium is taken to be unchanged from the pure monomer. This situation is a reasonable approximation if the monomer is the predominant component of the photopolymerizable material and if its optical properties (and density) are insensitive to conversion. In this case of ideally photo-invariant polymerization, the conversion fraction equals,

$$\phi(x,t) = 1 - \exp[-KI_0 \exp(-\mu_0 x)t]. \tag{8}$$

(Curiously, $1-\phi(x,t)$ is the Gumbel function [24] of extreme value statistics.) Eq. (8) can be written in the coordinate frame z of the moving front as,

$$\phi(x,t) = 1 - \exp[-\exp(-z)], \tag{9a}$$

$$z \equiv (x - x_p), \quad x_p = \ln(KI_0 t) \tag{9b}$$

As mentioned in the last section, the position of the FPP front can also be defined through the threshold condition for $\phi(x,t)$ and it is this type of front definition that is more convenient in the discussion of our measurements. Specifically, we define the height $h(t)$ of the FPP front by the condition $\phi(x,t) = \phi_C$:

$$h(t) \equiv x(\phi = \phi_C) \tag{10}$$

so that $\phi_c = 1 - \exp[-KI_0 \exp(-\mu_0 h)t]$. Thus, we may infer that the height $h(t)$ of the front grows logarithmically with time, as in the case of x_p,

$$h(t, \mu_0, KI_0, \phi_c) = \frac{\ln(t/\tau)}{\mu_0}, \tag{11a}$$

$$\tau(KI_0, \phi_C) \equiv \frac{\ln[1/(1-\phi_C)]}{KI_0}. \tag{11b}$$

The expression for $h(t)$ in Eqs. (11a) and (11b) is restricted to $t > \tau$ since the solidification front does not form instantaneously with light exposure. An induction time τ is required for ϕ to first approach ϕ_c and for the front to begin propagating. Notice that the slope of $\ln(t)$ factor, describing the growth of $h(t)$ in Eq. (11a) and (11b), depends only on the optical attenuation μ_0 rather than the rate of reaction and that the intercept governing the initial front growth is governed by τ which depends on the rate constant, optical intensity and ϕ_c. Traveling wavefronts with a logarithmic displacement in time occur in diverse contexts [25].

The transmission $\mathrm{Tr}(x,t)$ does not evolve in time photo-invariant polymerization so that $\mathrm{Tr}(x,t)$ simply decays exponentially with depth (x) according to Beer–Lambert relation, $\mathrm{Tr}(x,t) = \exp(-\mu_0 x)$.

It is important to realize that Eq. (11a) and (11b) describes the initial FPP growth for an arbitrary optical attenuation of the polymerized material. ($\mu_\infty > 0$). Moreover, Eq. (11a) and (11b) describes the long time asymptotic growth provided that μ_∞ is replaced by its non-vanishing counterpart μ_∞ for the fully polymerized material. These extremely useful approximations arise simply because $\mu_\infty(x,t)$ is slowly varying in these short and long time limits. The crossover between these limiting regimes can be non-trivial and is addressed below. In many practical instances, however, the time range is restricted to the initial stage governed by Eq. (11a) and (11b).

4.3. Partial photobleaching ($\mu_0 > 0$, $\mu_\infty < \mu_0$)

The limits of perfect photobleaching and photo-invariant polymerization are ideals that can only approximately apply in practice. In general, the optical attenuation of the polymerized material is always greater than zero and can be either greater or lesser than the monomer. We first consider the case where μ_∞ small ($\mu_\infty = 10^{-4}\ \mathrm{mm}^{-1}$) so that a constant velocity front propagation occurs over an appreciable time. The initial optical attenuation constant μ_0 and ϕ_c are chosen to roughly match the magnitude found in the experiments described in the next section, $\mu_0 = 10\ \mathrm{mm}^{-1}$, $\phi_C = 0.02$ (or 2%) and $KI_0 = 1\ \mathrm{s}^{-1}$. Our approach must be numerical since Eqs. (1) and (2) are not readily solved analytically, despite their apparent simplicity of form. These results are obtained by a finite difference solution of Eqs. (1) and (2), using IGOR Pro 4 (WaveMetrics), in which depth and time intervals of $10^{-3} < x < 7.6$ mm and $10^{-3} < t < 250$ s were sampled in logarithmic increments.

The transmission in the case of partial photobleaching remains nearly exponential, but the surface from which the attenuation occurs translates into the material in the course of photopolymerization at a nearly constant rate. The conversion fraction $\phi(x,t)$ exhibits a simple sigmoidal form and translates uniformly in time with a shape that remains invariant in form, although the full front does not pass into the positive real axis until a sufficient time passes. In Fig. 4(c), we show the derivative $-\mathrm{d}\phi(x,t)/\mathrm{d}x$ as function of time, the position of the peak defining the front position and its height the peak the reciprocal interfacial width [Eq. (7)]. Finally, Fig. 4d shows the front positions as defined by ϕ_C and the inflection point in $\phi(x,t)$. The inset shows that front

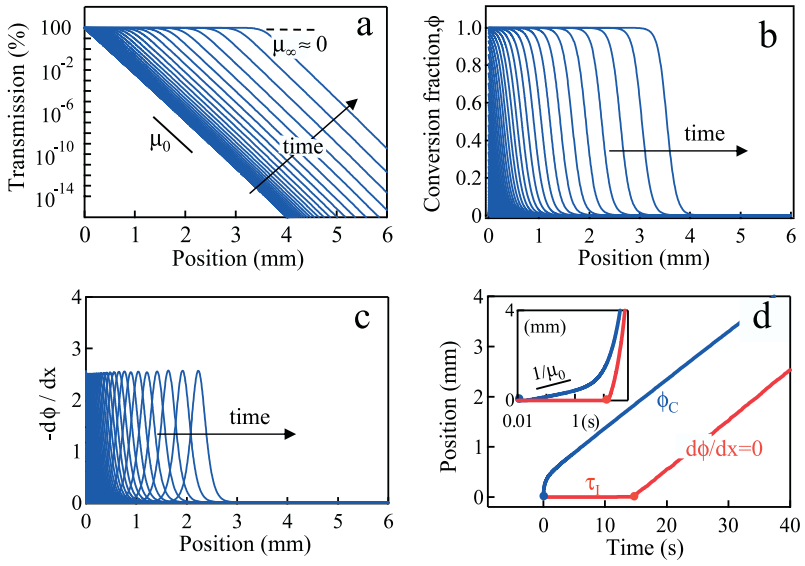

Fig. 4. Partial photobleaching. FPP front characteristics for partial photobleaching photopolymerization obtained numerically with parameters $\mu_0 = 10\ \mathrm{mm}^{-1}$, $\mu_\infty = 10^{-4}\ \mathrm{mm}^{-1}$, $KI_0 = 1\ \mathrm{s}^{-1}$ and $\phi_C = 2\%$ (time steps sampled logarithmically). (a) Transmission profile evolution, (b) Propagation of conversion profile, (c) Differentiated conversion profile, defining inflection point as measure of front position, (d) Front position obtained from inflection point position ($d\phi/dx = 0$) and height of the polymerized sample (obtained from critical conversion ϕ_C criterion). Note the front propagation is nearly linear in time at long times (since $\mu_\infty \approx 0$) for both the transmission and the conversion fraction and that the front shape is invariant in time, after an induction time. The height of the polymerization front (ϕ_C) exhibits non-trivial kinetic features (a log-to-linear crossover) that are absent from the kinetics defined by the inflection point in the conversion profile (which emanates after full conversion at the surface).

position as defined by the solidification front $h(t)$ grows logarithmically at short times, but the front propagation crosses over to linear growth at long times. The front defined by the inflection point, exhibits a different scenario. The front movement develops sharply at long times and propagates linearly at the outset. This effect arises since a fairly long induction time exists before the inflection point of ϕ passes onto the positive axis.

4.4. Partial photodarkening frontal photopolymerization ($\mu_0 > 0$, $\mu_0 < \mu_\infty$)

It is possible that the reactive products generated by the photoinitiator or the polymerization of the monomer to increase the optical attenuation so that the cross-linked material becomes increasingly opaque to (UV) radiation with increasing time. We find that this case is the most common situation in all of our FPP measurements, regardless of the presence of nanoparticles, or *T*. Fig. 5 illustrates our numerical solution obtained for a representative photo-darkening example using the realistic model parameters: $\mu_0 = 1\ \mathrm{mm}^{-1}$, $\mu_\infty = 10\ \mathrm{mm}^{-1}$, $KI_0 = 1\ \mathrm{s}^{-1}$ and $\phi_c = 0.02$ (or 2%), covering $10^{-3} < x < 20$ mm and $10^{-3} < t < 10^6$ s depth and time intervals in logarithmic increments. (Note how photobleaching growth of the network height $h(t)$ is much faster with similar physical parameters). The transmission $\mathrm{Tr}(x,t)$ as a function of depth for various curing times is computed in Fig. 5(a). In the short and long time limits, the usual Beer–Lambert law holds and the intensity decays exponentially in x, with attenuation coefficients μ_0 and μ_∞, respectively. At intermediate times, there is a crossover between these two asymptotic regimes. (An attempt to fit experimental transmission results with the simple Beer–Lambert law would result in an unphysical ($\neq 1$) intercept for infinitely thin films, symptomatic of the necessity of accounting for the variation in μ in the course of photopolymerization.) The spatio-temporal variation of the conversion fraction $\phi(x,t)$ is shown in Fig. 5b and the derivative $-\mathrm{d}\phi(x,t)/\mathrm{d}x$ of is shown in Fig. 5(c). As in the total photobleaching case, the front position as defined by the inflection point is insensitive to crossover effects because of the late time for the development of this feature. The displacement in time is logarithmic after a short induction time. However, the front position $h(t) \equiv x(\phi = \phi_c)$ defined by a 2% conversion exhibits a more interesting crossover. As anticipated from Eq. (5), the front moves logarithmically at 'short' times where $\bar{\mu}(x, t \to 0) \approx \mu_0$ and crosses over to a slope determined by $\bar{\mu}(x, t \to \infty) \approx \mu_\infty$, respectively, as the monomer interconverts to the network material. Thus, the front moves faster initially ($\propto 1/\mu_0$) and slows down ($\propto 1/\mu_\infty$) at later times.

5. Experimental results and discussion

In a previous paper [13], we investigated the comparison of the model described above to a series of commercially available thiol-ene PM formulations. These measurements compared quite favorably to our FPP model for the case of partial photodarkening. In the present work, we perform a

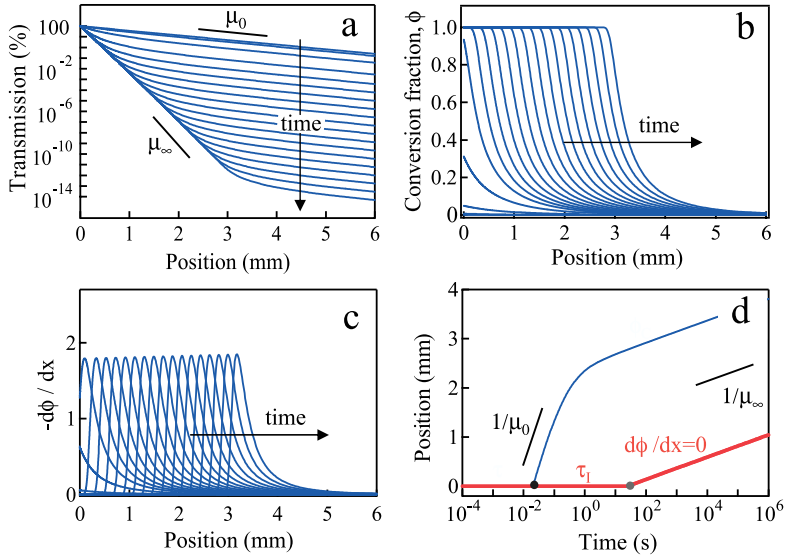

Fig. 5. Partial photodarkening FPP modeled numerically with parameters $\mu_0 = 1\ \mathrm{mm}^{-1}$, $\mu_\infty = 10\ \mathrm{mm}^{-1}$, $KI_0 = 1\ \mathrm{s}^{-1}$ and $\phi_C = 2\%$ (time steps sampled logarithmically). (a) Transmission profile evolution, (b) Propagation of conversion profile, (c) Differentiated conversion profile, with the inflection point demarking one measure of front position, (d) Comparison of front kinetics obtained by the inflection point position ($d\phi/dx = 0$) and critical conversion ϕ_C criteria. The latter corresponds to the position obtained experimentally from height of the polymerized sample. The attenuation coefficient μ increases in the course of time toward a well-defined larger value at large times, μ_∞. The time invariant FPP front moves logarithmically in time, in contrast with the linear kinetics of total photobleaching (Fig. 4). The height $h(t)$ exhibits two logarithmic dependences, after induction time τ: an early regime governed by the optical attenuation of the monomer (faster $1/\mu_0$) and a later regime governed by the optical attenuation of the polymerized material (slower $1/\mu_\infty$). The inflection point position departs after full conversion at the surface (induction time τ_I), moving with a $1/\mu_\infty$ logarithmic prefactor.

temperature study on one of these formulations (designated as r81 in our previous paper), and consider how the FPP process is modified by the presence of commonly utilized nanoparticles (silica, titania and (multi-wall carbon nanotubes).

5.1. FPP dependence on temperature

During photocuring, the initial homogeneous PM undergoes a complex spatio-temporal change, emanating from the illuminated surface and resulting in a depth- and time-dependent local transmission. It is important to first establish how the optical attenuation properties evolve in time so that we know what type of FPP formation should occur in our system. Measurements of the integrated transmission of specimens of constant thickness as a function of dose (Fig. 6(a)) indicate that the transmission progressively drops with exposure, corresponding to the case of photodarkening. The transmission dependence upon photocuring was studied by monitoring in-situ the transmitted light intensity of a layer of PM of constant thickness during FPP. Layers of pre-polymer were confined between transparent glass windows with spacers of defined dimensions: (90, 180, 198, 160, 400, 650, 1000 and 1475) μm. A large UV dose window was probed, ranging from 0.01 mJ/cm^2 to over 100 mJ/cm^2, and this experimental series was performed isothermally, at 20 °C. The inset shows fitted curves describing of thickness-dependent transmission before [Tr(0)] and after [Tr(∞)] a long UV exposure (until Tr(dose) reaches a plateau), in the usual Beer–Lambert representation. There is clearly a drop in μ in the photopolymerized material so that the partial photodarkening model applies to the data. Photodarkening of these PMs is caused by fluorescence emission in the visible range that is concurrent to photoinitiation and this effect will eventually disappear after even longer exposure times [26]. Further discussion of transmission characteristics of these FPP fronts are described in our previous paper [13]. Fig. 6(a) serves as a reminder here of this basic aspect of the FPP process in our thiol-ene PM.

Next, we discuss a series of combinatorial experiments carried out to determine the dependence of the patterned feature height $h(t)$ on the administered UV dose and temperature T. FPP was carried out through a photomask, consisting of an array of 10×10 squares (2 mm×2 mm), as described above. The T range investigated spanned from 16 to 73 °C, using two linear gradient samples. A thick layer (3 mm) of PM was then confined inside a PDMS gasket on a silicon wafer and covered with a glass slide and photomask. Each slit was UV exposed for increasing amounts of time using a sliding shutter at fixed light intensity. The top glass plate (where the cross-linked material is patterned) was then slowly lifted, leaving the majority of the uncross-linked material on the bottom surface. The uncross-linked material on the glass plate was removed upon development, and the patterned structures were flood UV exposed, as described above.

The temperature study was accomplished with only two combinatorial samples, each with 100 distinct experimental data points, defined by parameters (dose, T). The two

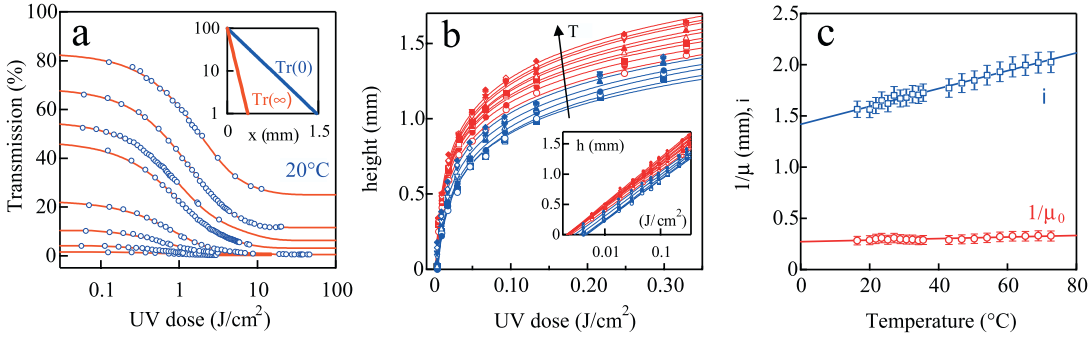

Fig. 6. Influence of temperature on 'photodarkening' FPP kinetics. (a) Transmission change during light exposure for various sample thicknesses, ranging from 90 μm to 1 mm (measured at 20 °C), establishing the photodarkening nature of the process. The inset depicts a Beer–Lambert plot (log transmission as a function of thickness) the initial and final stages, yielding parameters μ_0 and μ_∞. (b) Frontal kinetics measured at several temperatures (5% standard uncertainty) obtained from two combinatorial specimens, linearly sampling (16–34) °C and (36–73) °C. The lines are logarithmic fits to individual sets of data, demonstrating the validity of log frontal kinetics which is accelerated with increasing temperature. The inset replots the measurements in a semi-log representation establishing that slope (i.e., logarithmic prefactor) is largely unchanged, while the intercept decreases with increasing temperature. (c) Fitting parameters of measurements in (b) to a logarithmic growth law $h(\text{dose}) = i + (1/\mu_0)\ln(\text{dose})$, where i stands for intercept (Eqs. (12a) and (12b)). Temperature effects are manifested primarily by an increase in the intercept i, which is a function of the kinetic constant K and critical degree of conversion ϕ_C, while the slope is controlled by the optical attenuation μ_0 in the photodarkening FPP model.

T-gradients were mapped into $T(p) = 0.3152p + 16.4$ °C and $T(p) = 0.653p + 35.64$ °C, where p stands for sample position along the gradient ($0 \le p \le 56.6$ mm). The gradient linearity was better than the regression parameter $R^2 > 0.99$. The temperature T of each sample was interpolated from the expression above and has an uncertainty better than 0.5 °C. The exposure times ranged from 30 s to 37 min, and the light intensity was (230–245) μW/cm^2, thus covering a 4–330 mJ/cm^2 dose window (with 5% standard uncertainty based on one standard deviation). The resulting patterned posts were topographically mapped by profilometry and the front position (i.e., the maximum height) was also measured with a caliper (Fig. 3). Our method of locating the 'cure depth' or 'front position' $h(t)$ is tangibly defined measuring the thickness of the solidified material after UV exposure and subsequent development (washing away the unsolidified thiol-ene PM). This criterion [13,27] is suitable for characterizing and controlling feature depth in fabrication and prototyping since the dimensions of the solid material are the primary concern.

In the present paper, we use UV dose (the product of exposure time and light intensity, dose $\equiv I_0 \times t$) and time t almost interchangeably. This relation is established from Eq. (1), which is invariant under the formal replacement, $t =$ dose/I_0. As a control measurement in our previous work [13], we carried out cure depth h experiments with various fixed incident light intensities I_0 and exposure time intervals t and found that all the data superimposed using the time–dose relation. Thus, the conversion rate does not appear to depend on I_0 [4,27].

Fig. 6b collects height $h(t)$ vs. dose experimental observations for a range of T for the thiol-ene PM. The data shows that $h(t)$ grows more rapidly at elevated T and the inset compares the growth is effectively logarithmic in each case, consistent with the photodarkening model. The time regime here does not extend to long enough times [13] to attain the crossover observed in Fig. 5(d). The patterned height grows, therefore, logarithmically with time, which is interpreted within the first growth regime of our photodarkening model [similar to photo-invariance Eq. (11a) and (11b)], according to

$$h(\text{dose}) = 1/\mu_0 \ln(\text{dose}) + i, \tag{12a}$$

$$i = -\ln\left[\frac{\ln[1/(1-\phi_C)]}{K}\right]/\mu_0. \tag{12b}$$

as discussed in Section 4.2. We observe from the inset of Fig. 6(b) that the slopes of the curves are nearly invariant to changes in T, but the intercept i changes. This result is expected from our FPP model since the slope of the logarithmic growth is entirely determined by the optical attenuation constant μ_0. The intercept i depends on the rate constant and the critical conversion fraction ϕ_C, both of which should depend on T. A fit of the data to the FPP model indicates supports these predictions of the FPP model, the slope of the logarithmic curves is nearly constant $1/\mu_0 \approx 0.31$ mm, corresponding to $\mu_0 \approx 3.2$ mm^{-1} (which appears to decrease slightly with temperature, likely associated to a decrease in density). The intercept increases nearly linearly with T over this limited T range, following $i \approx 0.0085T + 1.4336$. The data could be fitted to an Arrhenius form expected for the rate constant K, but we avoid this procedure until we have a better understanding of the T dependence of ϕ_C. These observations show that the FPP model can be used to understand the T dependence of FPP and the parameters governing the photopolymerization process. At even high T and light dose (typically above 65 °C and 250 mJ/cm^2) the planarity of front propagation appears to be somewhat disrupted, likely due to frontal instabilities that we will report separately [28].

The T dependence of i rationalizes the qualitative observations of Fig. 2(a): posts patterned with low UV

dose at lower temperatures were washed away upon development, indicating the existence of a critical dose for the frontal polymerization to initiate.

The frontal kinetics of a FPP material is defined by only four parameters in the framework of our model: μ_0, μ_∞, K and ϕ_C. The attenuation coefficients can be determined independently with a set of Tr vs. thickness experiments of the neat and fully polymerized material (Fig. 6(a)). K may be determined by the time (or dose) dependence of the Tr, for various thicknesses. Finally, the conversion threshold ϕ_C is obtained by fitting the experimental height vs. dose measurements. We previously obtained [13] $K=0.55$ cm^2/J and $\phi_C=0.32\%$ for this thiol-ene PM formulation at $T=20$ °C.

5.2. FPP with nanoparticles

Next, we demonstrate the applicability of the FPP model to the case when small amounts of nanoparticles are added to the thiol-ene PM. This series of measurements was performed at constant T ($T=25$ °C), following the same experimental protocol as the neat thiol-ene PM. An array (3×9) photomask was employed and light exposure was varied in both directions (instead of temperature) with a double shutter, following the sequence indicated in Fig. 2(b). Particle loading varied from 0.01 to 1% and its upper limit was set by a decreasing light transmission, which lengthens experimental time. Measurements were performed for a range of common nanoparticle additives-silica, titania and multiwall carbon nanotubes-known for their capacity to modify mechanical, conductivity and optical properties.

The impact of the filler additives on the front development is shown in Fig. 7. As in the thiol-ene matrix alone, the growth remains logarithmic in all cases. The primary effect of the nanoparticle additives is to modify the slope of the logarithmic growth. This result is expected since the filler particles modify the optical attenuation of the medium, which governs the slope of the logarithmic growth according to the FPP model. The slope change is smallest for the silica particles (1% mass fraction) and the dilute (0.01%) nanotube dispersions, but the effect becomes quite pronounced for higher concentrations of CNT (0.1%) and titania (1%) particles, where the changes in the optical properties are strongly modified. In fact, the optical attenuation of the media may be determined by the frontal kinetics alone, from the logarithmic growth slope. Accordingly, we obtain μ (1% SiO_2) ≈ 4.3 mm^{-1}, μ (1% TiO_2) ≈ 36.0 mm^{-1}, μ (0.1% CNT) ≈ 18 mm^{-1}, μ (0.01% CNT) ≈ 5.0 mm^{-1}.

Our FPP model seems to provide a good description of these multicomponent mixtures, despite the microheterogeneity of the photopolymerizable material. We have previously demonstrated the use of FPP in 3D rapid prototyping (3D-RP) and fabrication of complex structures, with particular emphasis in microfluidics [5,13,29–31]. The addition of nanoparticles emerges as a useful method to modulate the rate of FPP and opens possibilities in 3D-RP of structures with varied material properties, such as optical elements, wires, electrodes, resistors and other circuit elements, etc. The present results are quite encouraging for device manufacture and suggest a wide applicability of our FPP model.

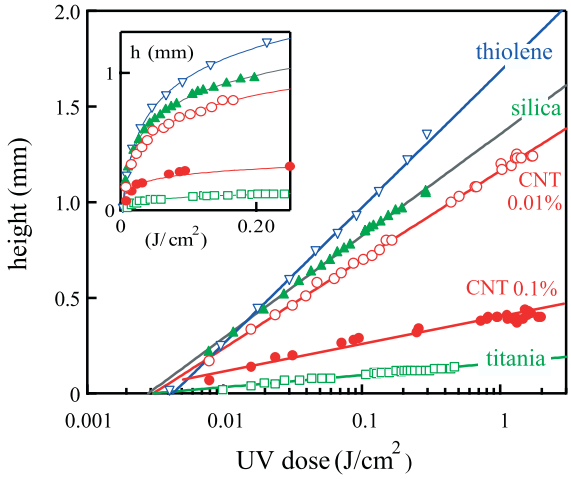

Fig. 7. Influence of nanoparticle additives on 'photodarkening' FPP. Isothermal (25 °C) frontal kinetics of the neat (▽) thiol-ene matrix is considerably slowed down in presence of mass fractions: (▲) 1% silica, (□) 1% titania, (●) 0.1% CNT and (○) 0.01% CNT nano-fillers (average height uncertainty is less than 5%, measured by one standard deviation). The primary effect of the additives is to decrease the logarithmic slope describing the FPP growth. This effect is expected from our model in which the optical attenuation alone (in fact, $1/\mu_0$) governs that slope. The strong optical attenuation of carbon nanotubes and titania slow down growth more efficiently, as anticipated. Our FPP model successfully describes frontal growth in these multicomponent mixtures, despite the microheterogeneity of the photopolymerizable material.

6. Conclusions

We have developed a model frontal photopolymerization (FPP) that directly addresses the kinetics of the growth front position and the change in optical attenuation in time under general circumstances, including the variation in temperature and loading with nanoparticles to change the properties of the photopolymerized material. This model involves an order parameter $\phi(x,t)$ describing the extent of conversion of monomer to polymer (solid) and the extent of UV attenuation, $\mathrm{Tr}(x,t)$. Many aspects of the photopolymerization process derive from the changing character of the optical attenuation μ in the course of PM exposure to UV light and we illustrate how this effect can lead to significant changes in the kinetics of front propagation. Specifically, the fronts are observed to propagate linearly in time, when μ of the polymerized material is very small (photobleaching), while a logarithmic front growth is found for photopolymerization when the optical attenuation remains nearly unchanged (photo-invariant FPP).

In the measurements described in the present paper, we generally observe an increase in the optical attenuation in time (partial photodarkening). A series of combinatorial experiments with varying temperature demonstrates that the front height generally increases with temperature and is well described by logarithmic growth at all T. The log prefactor is found to be nearly independent of temperature, while the induction time for FPP initiation increases with T. This is consistent with our model, which predicts that the log prefactor depends entirely on the optical attenuation at short times (relevant to the measurements considered) and the induction time is temperature dependent, primarily through the rate constant, K.

We also explored the influence of nanoparticles on FPP growth and found that logarithmic kinetics is preserved. However, the slope on the log prefactor depends strongly on nanoparticle type and concentration but the induction is largely unchanged. These findings are consistent with our FPP model. These two series of measurements show that the FPP growth can be independently tuned by either modifying the rate constant (e.g., by varying T or the formulation [13]) or optical properties (e.g., nanoparticle additives) of the PM. Our experimentally validate FPP model should be a useful tool in the design and fabrication of diverse multicomponent structures by FPP.

Acknowledgements

We acknowledge Joseph Antonucci (NIST) and Eric Grulke (University of Kentucky) for kindly donating the titania and silica nanoparticles and multiwall carbon nanotubes. We thank Vladimir Entov (Russian Academy of Sciences), James Warren (NIST) and Fern Hunt (NIST) for helpful discussions on the modeling of FPP and Brandon Vogel (NIST) for assistance during experiments. We especially thank James Warren for his help in identifying inaccuracies in the numerical computations of the conversion fraction in Section 4. Support from the NIST Combinatorial Methods Center (NCMC) is greatly appreciated.

References

[1] Odian G. Principles of polymerization. New York: Wiley; 1991.
[2] Fouassier J-P. Photoinitiation, photopolymerization, and photocuring. Cincinnati, OH: Hanser/Gardner Publications; 1995.
[3] Fouassier J-P, Rabek JF, editors. Radiation curing in polymer science and technology. London: Elsevier Applied Science; 1993.
[4] (a) Decker C. Polym Int 1998;45:133.
(b) Decker C. Polym Int 2002;51:1141.
[5] Harrison C, Cabral JT, Stafford C, Karim A, Amis EJ. J Microeng Micromach 2004;14(153):13. See also Ref. [13].
[6] (a) Khan AM, Pojman JA. Trends Polym Sci 1996;4:253.
(b) Pojman JA, Ilyashenko VM, Khan AM. J Chem Soc, Faraday Trans 1996;92:2825.
(c) Lewis LL, DeBisschop CA, Pojman JA, Volpert VA. In: Pojman JA, Tran-Cong-Miyata Q, editors. Nonlinear dynamics in polymeric systems. ACS symposium series, vol. 869, 2004. p. 169.
[7] Rytov BL, Ivanov VB, Ivanov VV, Anisimov VM. Polymer 1996;37:5695.
[8] (a) Terrones G, Pearlstein AJ. Macromolecules 2001;34:8894.
(b) Terrones G, Pearlstein AJ. Macromolecules. 2001;34:3195.
(c) Terrones G, Pearlstein AJ. Macromolecules 2003;36:6346.
(d) Terrones G, Pearlstein AJ. Macromolecules 2004;37:1565.
[9] Ivanov VV, Decker C. Polym Int 2001;50:113.
[10] (a) Goodner MD, Bowman CN. Macromolecules 1999;32:6552.
(b) Goodner MD, Bowman CN. Chem Eng Sci 2002;57:887.
(c) O'Brien A, Bowman CN. Macromolecules 2003;36:7777.
[11] Miller GA, Gou L, Narayanan V, Scranton AB. J Polym Sci, Part A: Polym Chem 2002;40:793.
[12] Belk M, Kostarev KG, Volpert V, Yudina TM. J Phys Chem B 2003;107:10292.
[13] Cabral JT, Hudson SD, Harrison C, Douglas JF. Langmuir;20:10020.
[14] Certain commercial equipment, instruments, or materials are identified in this paper in order to specify the experimental procedure adequately. Such identification is not intended to imply recommendation or endorsement by the National Institute of Standards and Technology, nor is it intended to imply that the materials or equipment identified are necessarily the best available for the purpose.
[15] Jacobine AF. in Ref. [3], Vol. 3, Chapter 7.
[16] (a) Cramer NB, Scott JP, Bowman CN. Macromolecules 2002;35:5361.
(b) Cramer NB, Davies T, O'Brien AK, Bowman CN. Macromolecules 2003;36:4631.
(c) Cramer NB, Reddy SK, O'Brien AK, Bowman CN. Macromolecules 2003;36:7964.
(d) Reddy SK, Cramer NB, Cross T, Raj R, Bowman CN. Chem Mater 2003;15:4257.
[17] Andrews R, Jacques D, Rao AM, Derbyshire F, Qian D, Fan X, et al. Chem Phys Lett 1999;303:467.
[18] Meredith JC, Smith AP, Crosby AJ, Amis EJ, Karim A. Combinatorial methods for polymer science. Encyclopedia of polymer science and technology. New York: Wiley; 2002.
[19] Wegscheider RZ. Phys Chem CIII 1923;103:273.
[20] Mauser HZ. Naturforsch B 1967;22:569.
[21] Warren JA, Boettinger W. Acta Metall Mater 1995;43:689.
[22] Ferreiro V, Douglas JF, Warren JA, Karim A. Phys Rev E 2002;65:051606.
[23] Warren JA, Cabral JT, Douglas JF (submitted).
[24] (a) Gumbel EJ. Statistics of extremes. New York: Columbia University Press; 1958.
(b) Galambos J. The asymptotic theory of extreme order statistics. Malabar, Fl: R.E. Krieger Publishing Co.; 1987.
[25] Ben-Naim E, Krapivsky PL, Majumdar SN. Phys Rev E 2001;64:135101. Majumdar SN. Phys Rev E 2003;68:026103.
[26] Personal communication by E. Norland of Norland Products, Inc., New Brunswick, NJ.
[27] Hirose T, Wakasa K, Yamaki MJ. Mater Sci 1990;25:1209.
[28] Cabral JT, Douglas JF. (unpublished work).
[29] Wu T, Mei Y, Cabral JT, Xu C, Beers KL. J Am Chem Soc 2004;126:9880.
[30] Hudson SD, Cabral JT, Goodrum W, Beers KL, Amis EJ. (submitted for publication).
[31] Cygan ZT, Cabral JT, Beers KL, Amis EJ. Langmuir (in press).